INTERNATIONAL JOURNAL FOR NUMERICAL AND ANALYTICAL METHODS IN GEOMECHANICS
Int. J. Numer. Anal. Meth. Geomech., **23**, 1319–1335 (1999)

A GENERAL MODELLING OF EXPANSIVE AND NON-EXPANSIVE CLAYS

J. C. ROBINET[1], M. PAKZAD[1], A. JULLIEN[1]* AND F. PLAS[2]

[1]*Euro-Geomat Consulting, 51, route d'Olivert, 45100 Orléans, France*
[2]*Agence nationale pour la gestion des déchets radioactifs (ANDRA), Parc de la croix blanche 1/7, rue Jean-Monnet, 92298 Chatenay-Malabry Cedex, France*

SUMMARY

This paper presents an elastoplastic model for saturated expansive and non-expansive clays. The original feature of this model is that a plastic mechanism is introduced during unloading to take into account the irreversible swelling of the macroporosities. These strains are induced by the repulsive stresses which are unbalanced at the scale of the microporosities. Thus two yield surfaces are activated: a classical contact yield surface (F_C) similar to an associated modified Cam-clay approach and a swelling yield surface (F_{R-A}) based on the non-associated plasticity. The formulation considers that for the normally consolidated stress states, the strains are mainly produced by an increase of the contact stresses. For the overconsolidated stress states, the repulsive stresses balance the external stresses. The rheological parameters are easily determined from the results of either triaxial or oedometer tests. The model is then used in a finite element program, using the classical concepts of plasticity, especially for the loading–unloading criterion based on the sign of the plasticity multiplier. Simulations of the convergence of a gallery (under an earth retaining structure) sunk at great depth in Boom clay are presented. The results are compared with those obtained with the Cam-clay model.

KEY WORDS: elastoplastic model; expansive clay; repulsive stress; contact stress; finite element method; gallery

INTRODUCTION

Classically, modelling of the swelling behaviour of clay soils was developed on the basis of a swelling pressure obtained from the laboratory oedometer tests.[1] However, the strong dependency of this pressure upon the loading path was noticed.[2] On the other hand, Mitchell[3] and Sridaharan[4] extended the concept of Terzaghi's effective stresses in order to describe the stress–strain behaviour of expansive clays postulating that, the strains are defined by the following stress states: σ'_C the effective contact stress, u_w the interstitial pressure and σ_{R-A} the internal stress resulting from the attractive and repulsive forces. Thus $\sigma = \sigma'_C + u_w + \sigma_{R-A}$.

Usually, the hydromechanical behaviour of clays is governed by interparticular interactions: the attractive and repulsive forces, the interstitial fluid pressure and the interparticular friction

*Correspondence to: A. Jullien, Euro-Geomat Consulting, 51, route d'Olivert, 45100 Orléans, France

CCC 0363–9061/99/121319–17$17.50
Received September 1996
Revised 14 December 1998

forces. The model developed by Derjaguin and Landau[5] and by Verwey and Overbeek,[6] called DLVO, is usually used to describe the stability of colloidal suspensions charged with particles. In this model four kinds of interactions are considered: thermal agitation, very short-range repulsive forces, Van der Waals attractive forces and double-layers repulsive forces. Ensuring that some specific effects are taken into account, the model is still available when long-range interparticular interactions are considered. Thus, the micro–macro transform to describe macroscopic swelling using the DLVO model is quite automatic under diluted regimes while for concentrated regimes it cannot really be applied.

Dormieux *et al.*[7] describe macroscopic swelling from the double-layer theory and use a relationship between the coefficient of a poroelastic model and the microscopic laws. But, despite important mathematical investigations, only partial results are obtained. From cyclic experiments on the bentonite Mx-80, Börgesson *et al.*[8] point out a strong hysteresis of the stress–strain curves. The behaviour is described through a macroscopic approach with an elastoplastic model using a Drucker–Prager failure criterion. Swelling is described by an important decrease of the Young modulus during unloading. Finally, Giraud *et al.*[9] have proposed a visco-elastoplastic model to evaluate the effects of the delayed convergence in the underground works built in Boom clay which is expansive.

In this paper, we present an elastoplastic model based on the strain mechanisms of the textures of saturated expansive clays under ambient temperature conditions.

MECHANICAL BEHAVIOUR OF EXPANSIVE AND NON-EXPANSIVE CLAYS

Oedometer and isotropic tests

Figure 1 presents the oedometric behaviour of an expansive clay—a smectite—and of a non-expansive clay—a kaolinite—(Table I). The experiments are carried out using a 1 MPa water back pressure. The samples are obtained from a paste which is consolidated up to 25 MPa for the smectite and up to 13 MPa for the kaolinite. The experimental consolidation slopes are same. But during unloading the smectite exhibits a much higher swelling strain than the kaolinite and shows a very wide hysteresis loop when reloading. Furthermore, Baldi's *et al.*[10] and Börgesson's *et al.*[8] experiments of Book clay and on a bentonite Mx-80 under overconsolidated conditions showed the following characteristics: (i) a strong variation of the consolidation slope associated with significant settlement strains, (ii) an important swelling when unloading which increases with the consolidation stress, (iii) a significant hysteresis loop along the loading–unloading–reloading cycle.

Triaxial tests

Rousset[11] performed two sets of overconsolidated drained triaxial tests: (i) the non-expansive clay of Couy taken at a depth of 337 m, under a 2 MPa confining pressure (OCR $\approx$ 4), (ii) the Boom expansive clay taken at a depth of 243 m, under a 1 MPa confining pressure (OCR $\approx$ 6). For the Couy clay a typical behaviour of overconsolidated non-expansive clays was observed: a significant dilatancy and a sudden drop of the deviatoric stresses. On the other hand, the behaviour of the slightly expansive Boom clay strongly differed from the former, especially: (i) the linear part of the behaviour was quite nil, (ii) strain hardening was mainly positive, characterized by contractant volumetric strains. The comparison between these results shows that the swelling

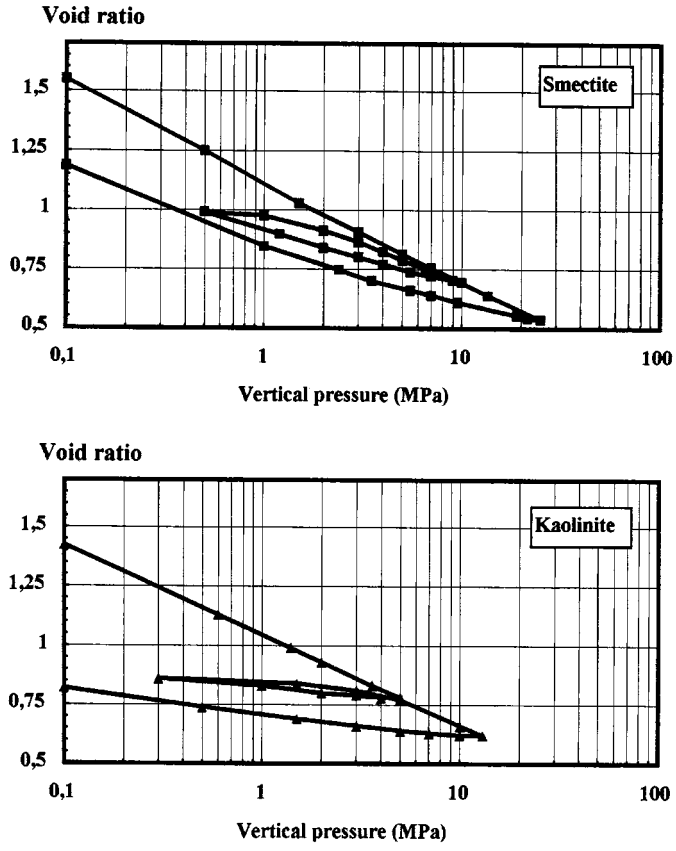

Figure 1. Cyclic oedometric tests on a smectite and on a kaolinite under different unloading consolidation pressures

Table I. Physical and mineralogical composition of the clays of the study

Characteristics	Smectite	Kaolinite	Boom clay
Grain density	2·75	2·65	2·67
Specific surface	426 m^2/g	10·3 m^2/g	53–177 m^2/g
Exchange capacity	64 meq/100 g	—	40 meq/100 g
Liquid limit	112%	40%	59–79%
Plastic limit	50%	20%	25–26%
Plasticity index	62%	20%	27–50%
Smectite/Kaolinite	(50/50) 80% ± 2	—	—
Kaolinite	4% ± 2	86% ± 3	30%
Geothite	6% ± 1	—	—
Calcite	2% ± 1	—	—
Quartz	6% ± 1	6% ± 1	28%
Feldspar and Mica	—	8% ± 1	—
Illite	—	—	20%
Smectite	—	—	22%

process occurring during unloading (overconsolidated material) leads to a loss of memory of an expansive clay.

Baldi *et al.*[10] performed many triaxial experiments under drained conditions, on natural Boom clay under various confining pressures. For either normally consolidated or slightly overconsolidated tests, a behaviour close to those of a non-expansive clay is noticed, especially a positive strain hardening. For highly overconsolidated tests, the volumetric strains remain contractant, although they are dilatant for a non-expansive clay. Moreover, an hysteresis loop in the $(q - \varepsilon 1)$ plane is observed when the material is unloaded and reloaded. The higher the deviatoric stress is when unloading, the more significant the hysteresis loop is.

ANALYSIS OF MICROSCOPIC MECHANISMS RESPONSIBLE FOR MACROSCOPIC SWELLING

The assembly of the basic structures (sheet–water) constitutes a disorderly medium inside which three kinds of pore spaces are found: interlamellar, interparticular and interaggregates. Some clays, which include very weak interlamellar bonds, fix the water molecules between two sheets. The water goes into the particles and get organized in monomolecular layers. This mechanism is associated with an intraparticular or interlamellar swelling[12] which produces a macroscopic swelling. Swelling is usually considered to be created by the excess of the repulsive osmotic pressure inside the adsorbed water molecules. This pressure which is the only internal stress which arises inside the particles, can reach 10 MPa.[13] Thus, the hydromechanical behaviour of saturated clays is controlled by several forces: (i) the solid–solid (skeleton–skeleton) forces, (ii) the interactions between the solid and liquid phases, and (iii) the attractive and repulsive electric forces (internal forces) between the particles.

The distribution of the internal forces in clay media was studied by Israelachvili *et al.*[14,15]. They found that in the case of non-expansive clays there is an equilibrium between the repulsive and attractive forces. The external stresses are then balanced by the contact stresses and by the interstitial pressure: $\sigma = \sigma'_{\mathrm{C}} + u_{\mathrm{w}}$. However, expansive clays are characterized by an excess of the repulsive forces with respect to the attractive forces while the former strongly depend on the molar concentration of the interstitial fluid. Thus, the presence of internal forces has to be taken into account for high-density expansive clays. That is why Mitchell[3] and Sridharan[4] have extended Terzaghi's concept of effective stresses. They assumed that the strains of expansive clays were controlled by three stress stress: σ'_{C} the contact stress, u_{w} the interstitial pressure and $\sigma_{\mathrm{R-A}}$ the internal stress resulting from the repulsive and attractive forces. Thus, for an expansive clay the external stresses are balanced by the superposition of the contract stresses, of the interstitial pressure and of the repulsive stresses: $\sigma = \sigma'_{\mathrm{C}} + u_{\mathrm{w}} + \sigma_{\mathrm{R-A}}$. The next point to be discussed is, for an applied stress path, whether the repulsive stresses are produced or not to balance an increase or a decrease of the external stresses.

An analysis based on the pore network variations after oedometer tests is first presented. Atabek *et al.*[16] studied by mercury porosimetry the pore distribution of a smectite powder compacted at a constant water content for three dry densities ($\rho d = 16$; 18·4 and 19·5 kN/m^3) A quasi bimodal distribution of the porosity was obtained with: a first mode around 30 Å linked to the interlamellar and interparticular microporosity; and a second mode around 100 μm linked to the interaggregate macroporosity. This distribution varies from a bimodal one in the case of low densities to a monomodal one for high densities. The same comments can be given for Boom

clay samples. Thus, compaction of these materials is obtained by the decrease of the volume of the macroporosities.

The different steps of mud consolidation are then analysed in the light of the experimental results of Figure 1. At the beginning of mud consolidation, all the pore spaces can change (interlamellar, interparticular and interaggregate) but consolidation goes on with a decrease of the size and of the volume of the macroporosities. Thus, considering that the decrease of the microporosities should be obtained: (i) without other interactions for a non-expansive clay, (ii) with a marked increase of the repulsive stresses for an expansive clay, the repulsive interactions, if any, should be observed on the stress–strain curves. But, as the oedometric consolidation slopes of the two clays (Figure 1) are parallel, the microporosities do remain stable. Thus, the external stresses variation only produce a variation of the contact stresses ($\delta\sigma'_{\mathrm{C}}$).

Finally, the phenomena during unloading and reloading were examined in the case of expansive clays. Internal stresses are created along such stress paths, when transient unbalanced effects between the repulsive stresses and the contact stresses are produced. The excess of repulsive stresses is balanced by the microporosities strains. The dilatancy of the micropores leads to aggregate swelling: the interaggregate spaces get reorganized. Thus, the strains of the microporosites (reversible) seem to act as a catalyst on the macroporosity strains (irreversible). The external stresses variations are then compensated by the variations of the repulsive and attractive stresses ($\delta\sigma_{\mathrm{R-A}}$).

PRESENTATION OF A MODEL FOR THE EXPANSIVE CLAYS

Activation of the plastic mechanisms

The model hypothesis were based on the above analysis of the strains of expansive clays produced by (i) $\delta\sigma'_{\mathrm{C}}$ for the normally consolidated states, (ii) $\delta\sigma_{\mathrm{R-A}}$ for the overconsolidated states. The stress variations were then associated with two independent plastic mechanisms expressed with two yield surfaces. The contact yield surface F_{C} of the modified Cam-clay type corresponds to $\delta\sigma'_{\mathrm{C}}$. The swelling yield surface $F_{\mathrm{R-A}}$, based on non-associated plasticity and combined isotropic and kinematics strain hardening, is elliptic and corresponds to $\delta\sigma_{\mathrm{R-A}}$.

Figure 2 shows the principle of activation of the yield surfaces along an oedometric path. During mud consolidation (path 0–1) both the contact and the repulsive stresses vary: the two plastic mechanisms combined with the F_{C} and $F_{\mathrm{R-A}}$ surfaces are activated. Going on loading along path 1–2–3 produces a reduction of the macroporosites: the mechanism corresponding to the surface F_{C} is the only one activated. Along the unloading path 3–4, the excess of repulsive stresses is balanced by the strains of the microporosities: the volume of the macroporosities increases and the activated plastic mechanism corresponds to the surface $F_{\mathrm{R-A}}$. When reloading (path 4–3) and until the preconsolidation pressure ($P'3$) is reached, the activated plastic mechanism corresponds to $F_{\mathrm{R-A}}$. Then, only one of those yield surfaces is activated at one time.

Figure 3(a) shows some details on the surface $F_{\mathrm{R-A}}$ when unloading. The surface is initialized and swells until the final unloading state is reached while it remains in contact with the surface F_{C} at a fix point (point 1). As for reloading, Figure 3(b) points tout that $F_{\mathrm{R-A}}$ is initialized at the actual stress state and swells but in the opposite direction until normally consolidated stress states are reached (point 4). Beyond this point (path 4–5) the surface F_{C} is again activated while $F_{\mathrm{R-A}}$ remains constant.

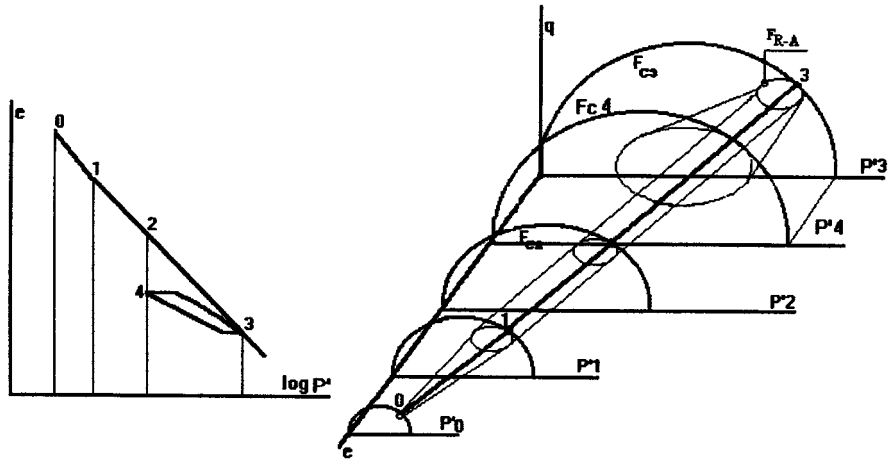

Figure 2. Schematic view of the two yield surfaces for an oedometric path along a loading–unloading–reloading cycle

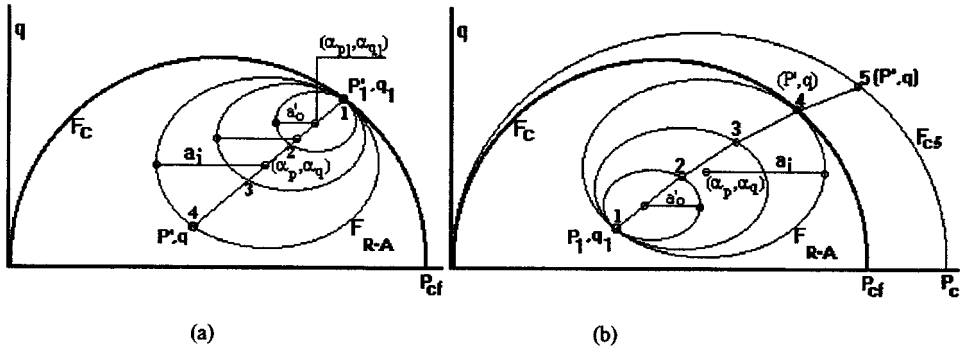

Figure 3. Schematic view of the activation of the F_{R-A} surface during: (a) unloading; (b) reloading

Constitutive equations

The elastic incremental behaviour is described using the formulation proposed by Hujeux:[17]

$$K = K_a P_a \left(\frac{P'}{P_a}\right)^n \quad \text{and} \quad G = G_a P_a \left(\frac{P'}{P_a}\right)^n \tag{1}$$

K and G in equation (1) are, respectively, the volumetric elastic modulus and the shear modulus which depend on the mean effective pressure (P') and on the initial moduli K_a and G_a.

The equation of the contact yield surface is given by

$$F_C = q^2 + M^2 \cdot P' \cdot (P' - P'_{Cf}) \cdot R^2(\theta) = 0 \tag{2}$$

P'_{Cf}, the preconsolidation pressure at the critical state is such that

$$P'_{Cf} = P'_{C0} \cdot \exp(\beta_1 \cdot \varepsilon_v^p) \tag{3}$$

In equation (3), P'_{C0} is the initial consolidation pressure, β_1 is the plastic compressibility modulus and ε_v^p is the strain hardening variable. $R(\theta)$ given in Eq. (2), θ being the Lode angle, is a function which allows for defining a failure criterion close to the Mohr–Coulombs' one:

$$R(\theta) = \frac{\sqrt{3}}{2} \cdot \frac{k1}{k1 \cdot \sin\theta + \cos(\pi/6 - \theta)} \quad \text{with } k1 \text{ a fitted parameter} \tag{4}$$

The equation of the swelling yield surface is

$$F_{R-A} = (q - \alpha_q)^2 + M^2 \cdot (P' - \alpha_p + a_i) \cdot (P' - \alpha_p - a_i) \cdot R^2(\theta) = 0 \tag{5}$$

α_p and α_q are the co-ordinates of the centre of the surface F_{R-A} and depend on the fix contact point (P'_1, q_1) of the two yield surfaces and on the actual stress state during unloading or reloading (P', q):

$$\alpha_p = \frac{P' + P'_1}{2}, \qquad \alpha_q = \frac{q + q_1}{2} \tag{6}$$

a_i in equation (5), the strain hardening parameter, is the major radius of the surface F_{R-A} and depends on the variables ε_v^p and ε_d^p associated with the yield of the surface. Thus

$$\mathrm{d}a_i = B_1 \cdot \mathrm{d}\varepsilon_v^p + B_2 \cdot \mathrm{d}\varepsilon_d^p \tag{7}$$

with

$$B_1 = P' \cdot \beta_2 \cdot \frac{\partial F_{R-A}/\partial P'}{-2\partial F_{R-A}/\partial a_i}, \qquad B_2 = M^2 \cdot P' \cdot \beta_2 \cdot \frac{\partial F_{R-A}/\partial q}{-2\partial F_{R-A}/\partial a_i},$$

At the initial state, a_i is equal to a_0 which is the initial radius of the surface (model parameter) and $\alpha_p = \alpha_{p1}$; $\alpha_q = \alpha_{p1}$. The plastic compressibility modulus at the overconsolidated state (β_2) is obtained with

$$\beta_2 = \beta_d = \beta_1 \cdot \left(1 + \frac{(P_C)_{ref}}{(P_C)_{dech}}\right) \cdot \frac{P_C}{P'} \quad \text{when unloading} \tag{8}$$

$$\beta_2 = \beta_r = \beta_1 \cdot \left(1 + \frac{(P_C)_{ref}}{(P_C)}\right) \cdot \frac{2P_{Cf}}{3(P_C)_{dech}} \cdot \frac{P'}{P_C} \quad \text{when reloading} \tag{9}$$

$(P_C)_{dech}$ in (8) and (9) is the critical unloading pressure and $(P_C)_{ref}$ is a reference value of the pressure in the model for swelling when unloading. Beyond $(P_C)_{ref}$, β_2 can be determined for any other unloading pressure. $(P_C)_{ref}$ corresponds to the pressure from which unloading in an oedometer test is done such that: $\beta_d = 2\beta_1$. The sign of the increment of the strain-hardening parameter $\mathrm{d}a_i$ allows to separate unloading from reloading (it must be positive). Thus, a negative value of $\mathrm{d}a_i$ during the loading path imposes to change the loading direction and to initialize a new yield surface F_{R-A}. Then, the plastic strains are given by

$$\mathrm{d}\varepsilon_v^p = \mathrm{d}\lambda_{R-A} \cdot \frac{\partial F_{R-A}}{\partial P'}, \qquad \mathrm{d}\varepsilon_d^p = \mathrm{d}\lambda_{R-A} \cdot \left(\frac{\partial F_{R-A}}{\partial q} - \alpha \cdot \frac{\partial F_{R-A}}{\partial P'}\right) \tag{10}$$

The parameter α which permits to define non-associated plasticity is obtained with

$$\alpha = \alpha_d = \left(1 - \frac{|P'_1 - \alpha_{p1}|}{a'_0}\right)\left(\frac{1{\cdot}5P_C}{(P_C)_{dech}} - 0{\cdot}5\right) \quad \text{when unloading} \tag{11}$$

$$\alpha = \alpha_r = \left(1 - \frac{|P'_1 - \alpha_{p1}|}{a'_0}\right)\left(1{\cdot}0 - 1{\cdot}5\frac{P_C}{P_{Cf}}\right) \quad \text{when reloading} \tag{12}$$

As for the plasticity multiplier ($d\lambda_{R-A}$) calculated from the consistency condition, it comes

$$d\lambda_{R-A} = \frac{\partial F_{R-A}/\partial \underline{\sigma}' \cdot \underline{\underline{C}} \cdot d\underline{\varepsilon}}{(\partial F_{R-A}/\partial P')^2(K + P'\beta_2) + \partial F_{R-A}/\partial q(3G + M^2P'\beta_2)(\partial F_{R-A}/\partial q - \alpha \cdot (\partial F_{R-A}/\partial P')} \tag{13}$$

TYPICAL PREDICTIONS ON LABORATORY PATHS

Eight rheological parameters have to be determined: (i) (K_a, G_a, n) for elasticity, (ii) (P'_{C0}, M, β_1) for the contact yield surface, (iii) (a_0, $(P_C)_{ref}$) for the swelling yield surface. The parameters used for the materials in this study are listed in Table II.

Table II. The rheological parameters used for simulations

	K_a	G_a	n	P'_{C0} (MPa)	M	β_1	a_0 (MPa)	$(P_C)_{ref}$ (MPa)
Boom clay	33	15	1	6·0	0·86	18	0·2	10
Bentonite Mx-80	11·1	3·7	1	8·2	1·0	10	0·35	10
Smectite	8·3	3·7	1	30	0·6	18	0·1	10

Modelling of oedometer tests

The oedometric stress path simulated with the two plastic mechanisms is drawn in the $q - P'$ plane on Figure 4. Thus, when unloading, the activation of the surface F_{R-A} is characterized by a high unloading slope and non-linear variations of the q/P' ratio. Figures 5 and 6 present a comparison between some experimental results and those predicted by the model, respectively, for the natural Boom clay and for the bentonite Mx-80. The cyclic loading paths show an important hysteresis loop which is well described by the model.

Modelling of drained triaxial tests

Figure 7 depicts the activation of the two plastic mechanisms for a drained triaxial stress path under overconsolidated conditions. The swelling yield surface F_{R-A} is first activated; the associated volumetric strains are contractant. Then, when the stress state becomes normally consolidated, both yield surfaces F_{R-A} and F_C are in contact and loading goes on which the activation of F_C. The strains depend on the contact point position of both surface. Volumetric dilatant strains are obtained in the field located above the line $q = MP'$. Below this line, the volumetric strains are contractant. Figures 8 and 9 present a comparison between the experimental results

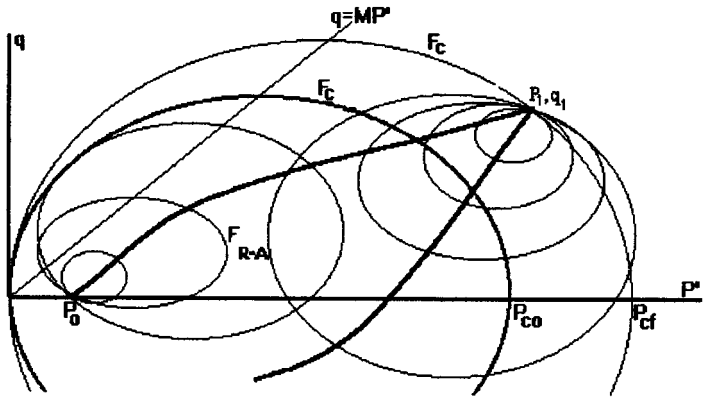

Figure 4. Schematic view of the activation of F_C and F_{R-A} surfaces on an oedometric path during a 'loading–unloading' cycle

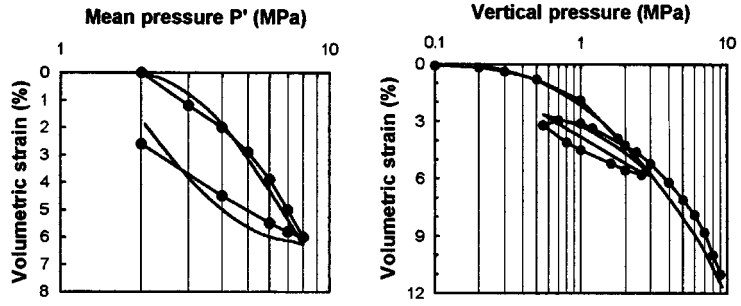

Figure 5. Comparison between the simulations and the experiments[10] on an oedometric path for the natural Boom clay

and those predicted by the model respectively, for a smectite and for the natural Boom clay. Contractance is observed for highly overconsolidated states; thus the higher the OCR, the wider are the hysteresis loops. Moreover, the unloading slope increases with the deviatoric unloading stress.

MODELLING OF THE TUNNELING OF A CIRCULAR GALLERY IN BOOM CLAY

The swelling model was implemented in a finite element code CLEO as well as the Cam-clay model to compare each prediction in the case of a groundwork. The excavation of an horizontal circular gallery, with a diameter of 6 m, at a depth of 250 m in Boom clay was simulated. Two analytical models (an elastic model and the elastic perfectly plastic Mohr–Coulomb's model) where first used in order to fix the mesh dimensions. The analytical calculations were done considering the following parameters: a constant isotropic initial stress of 5 MPa, a Young modulus of 500 MPa, a cohesion of 1 MPa, a slope of the critical state line of 0·86 and a friction angle of 22°. Figure 10 shows the vertical displacements predicted in the clay along the vertical axis above the gallery. At the wall of the gallery ($Y = 3$ m) the elastic model gives a displacement

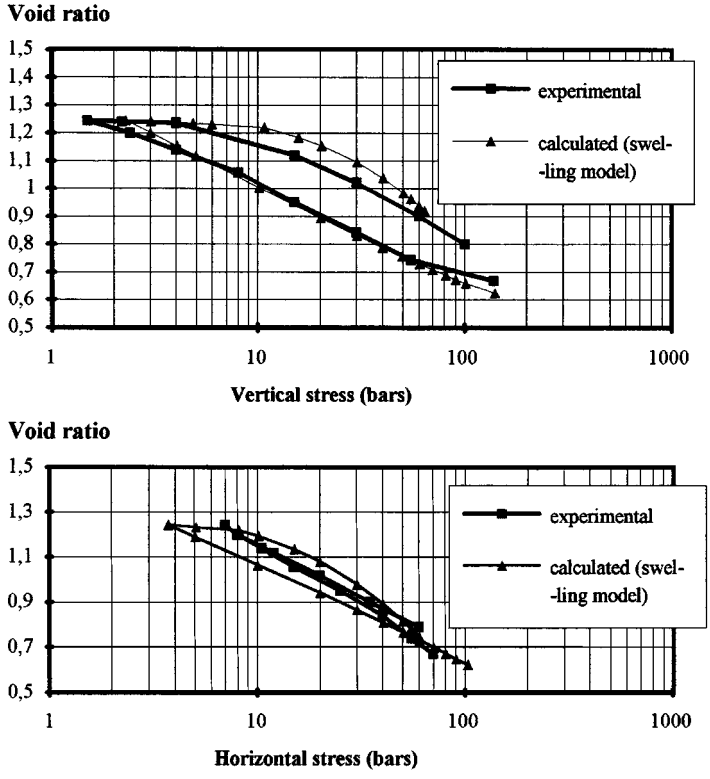

Figure 6. Comparison between the simulation and the experiment[8] on an oedometric path for the bentonite Mx-80

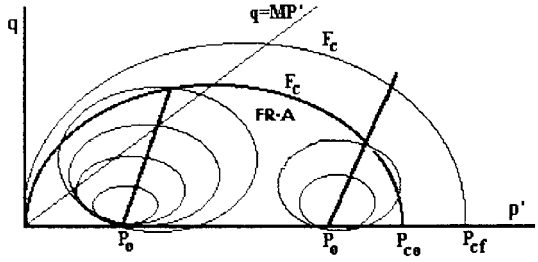

Figure 7. Schematic view of the activation of F_C and F_{R-A} surfaces on a drained triaxial path under slightly and highly overconsolidated conditions

of 4 cm and the Mohr–Coulomb's a value of 6·7 cm. Furthermore, at a distance of 20 m from the gallery centre, the displacement has significantly decreased.

Therefore, considering symmetry, half of the vertical section of a groundwork in a medium of 20 m × 20 m was studied. A plane strains finite element analysis was realized using the mesh of 72 isoparametric finite elements shown on Figure 11. The Boom clay parameters used for both the

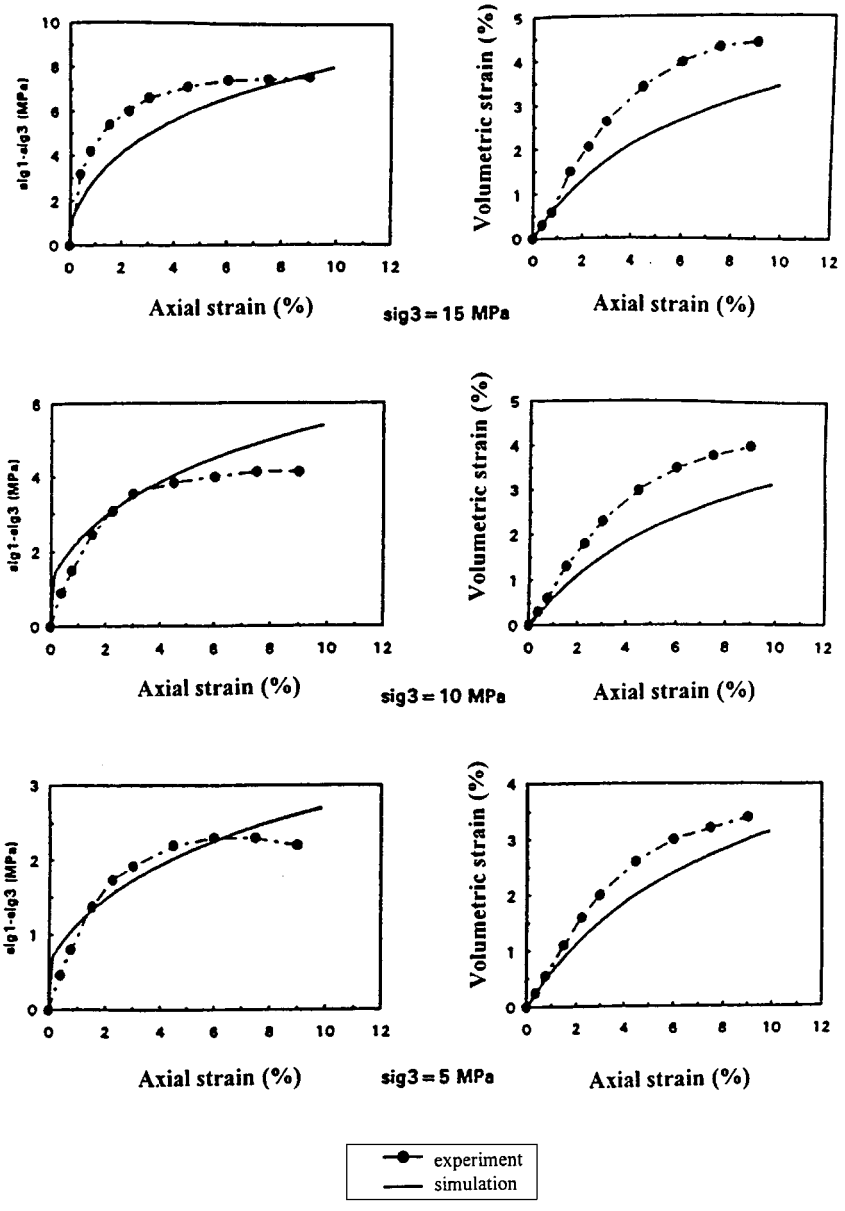

Figure 8. Comparison between the simulation and the experiment[18] on drained triaxial tests for a saturated smectite: (a) OCR = 2 (σ_3 = 15 MPa); (b) OCR = 3 (σ_3 = 10 MPa); (c) OCR = 6 (σ_3 = 5 MPa)

Cam-clay and the swelling models are those given in Table II. At the initial state, total normal stresses were applied to the contour of the gallery at the wall. The excavation was simulated by an incremental unloading until a zero normal stress at the wall was matched. The normal vector of each finite element at the wall of the gallery is inclined with an angle δ from the horizontal axis

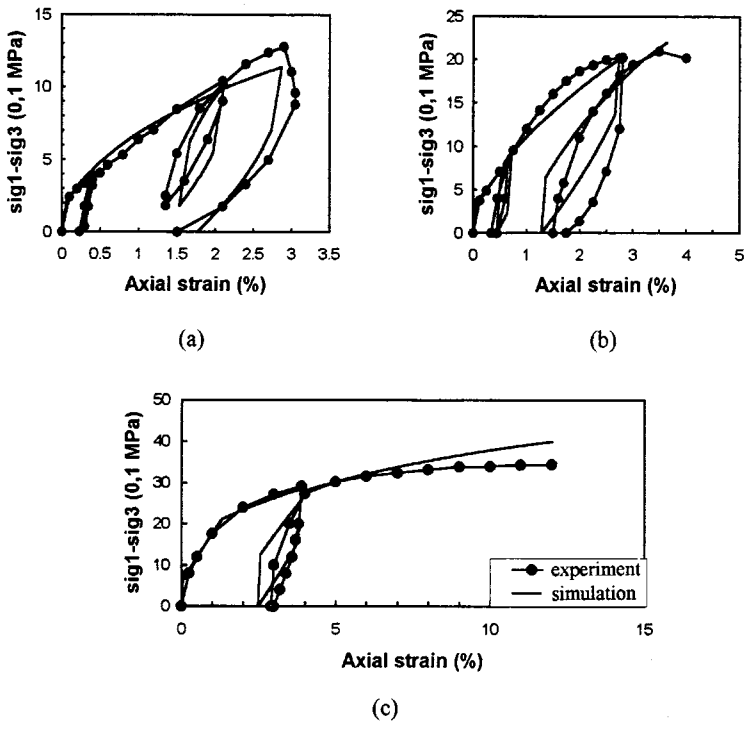

Figure 9. Comparison between the simulation and the experiment[10] on drained triaxial cyclic tests for natural Boom clay: (a) OCR = 7·5 (σ_3 = 0·8 MPa); (b) OCR = 3·0 (σ_3 = 2·0 MPa); (c) OCR = 1·5 (σ_3 = 4·0 MPa)

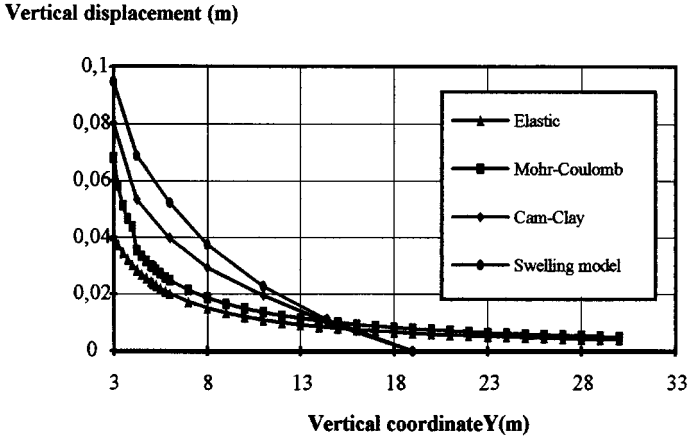

Figure 10. Vertical displacements obtained along the vertical axis of the medium above the gallery with analytical calculations (elastic and Mohr–Coulomb) and with numerical simulations (Cam-clay, swelling model)[19]

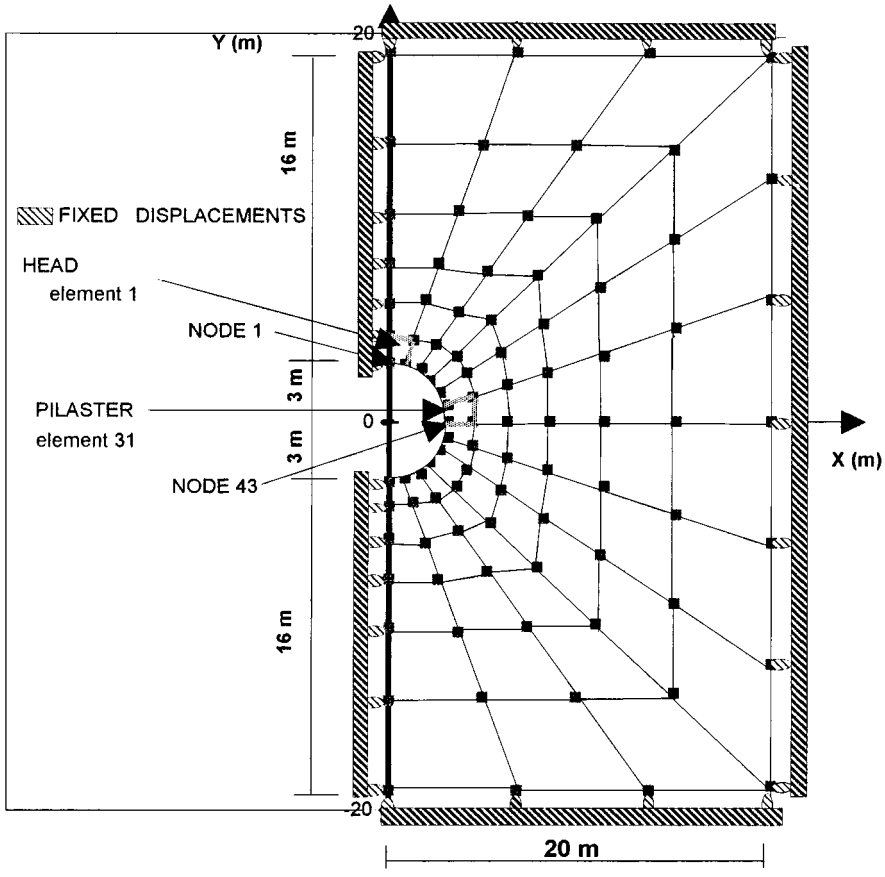

Figure 11. Mesh of the medium in the case of a circular gallery

Table III. Horizontal and vertical total stresses applied on the nodes of the gallery wall for $u_w = 2{\cdot}5$ MPa

δ	90°	82·51°	67·5°	52·47°	37·53°	22·51°	7·49°	0°
σ_n (MPa)	4·98	4·97	4·90	4.79	4.67	4.55	4.49	4.48
σ_{nx} (MPa)	0	0·65	1·88	2·92	3·70	4·21	4·45	4·48
σ_{ny} (MPa)	4·98	4·93	5·33	3·80	2·84	1·74	0·58	0

(X). Thus, the normal effective stress applied on a face inclined with an angle δ is given by

$$|\sigma'_n| = \sigma'_v \sqrt{\tfrac{1}{2}(1 + K_0^2) + \tfrac{1}{2} \cdot (K_0^2 - 1) \cdot \cos 2\delta} \tag{14}$$

Then, the horizontal and vertical components of the effective stresses are

$$\sigma' nx = \sigma' n \cos \delta, \qquad \sigma' ny = \sigma' n \sin \delta \tag{15}$$

Table IV. Final stresses at the walls of the gallery, at head stone (element 1) and at pilaster (element 31) with Cam-clay and with the swelling model[19]

Model	Element 1 (Head stone)			Element 31 (Pilaster)		
	σ_x (MPa)	σ_y (MPa)	σ_z (MPa)	σ_x (MPa)	σ_y (MPa)	σ_z (MPa)
Cam-clay	3·21	1·04	2·66	0·82	3·09	2·54
Swelling	3·25	1·09	2·26	0·86	3·16	2·17

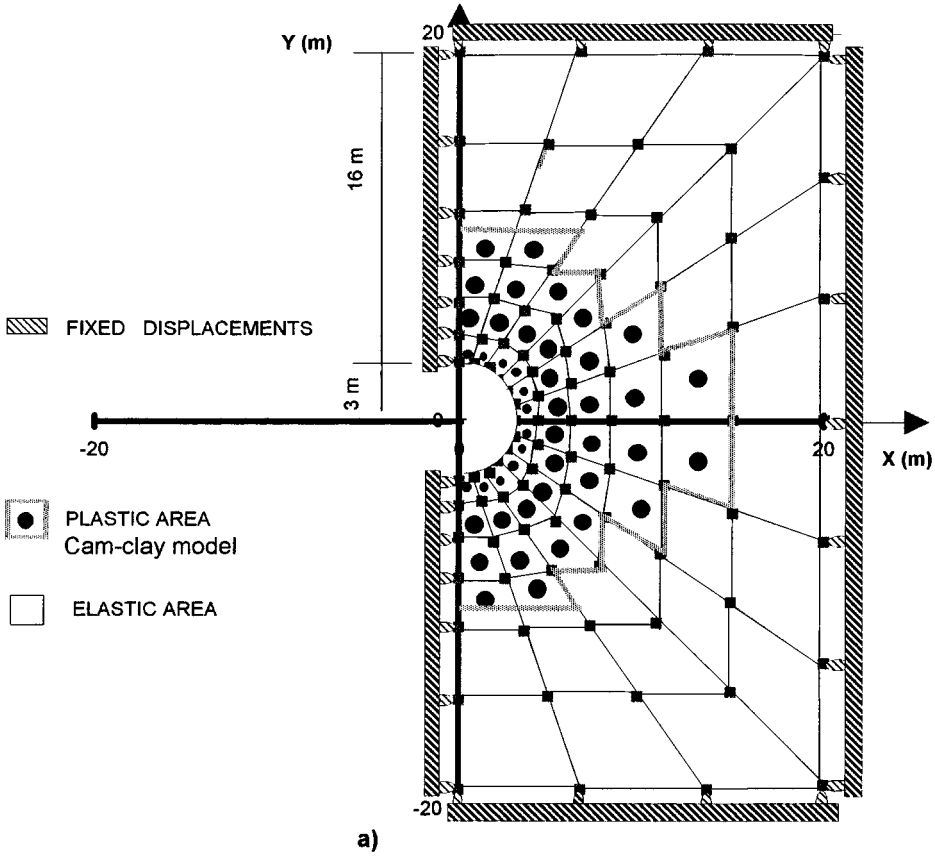

Figure 12. Presentation of the plastic area after deformation at the final unloading increment: (a) with the Cam-Clay model; (b) with the swelling model[19]

The components of the total stresses applied to the contour of the gallery (Table III) were determined from equation (15) and also with $\sigma_v = \sigma'_v + u_w$ ($u_w = 2{\cdot}5$ MPa) and $K0 = \sigma'_v/\sigma'_h = 0{\cdot}8$.

The numerical displacements along the vertical axis of the clay are also presented in Figure 10. Those predicted by the swelling model are significantly higher than those given by the Cam-clay

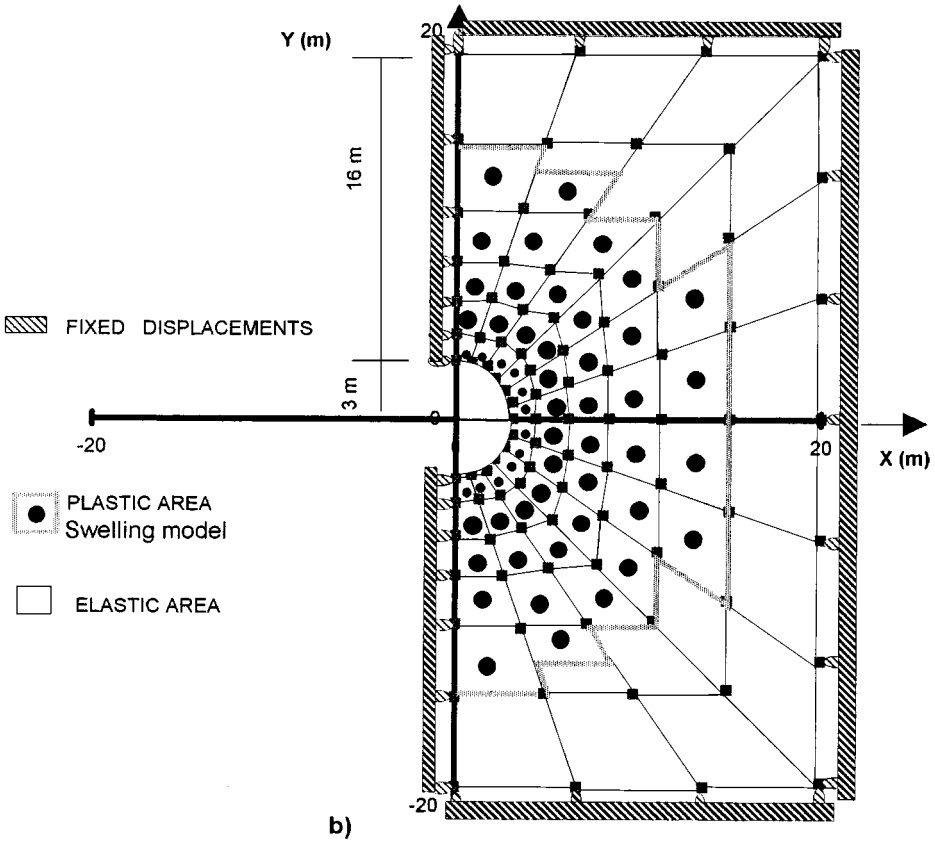

Figure 12. Continued

Table V. Displacements and final convergence values obtained with the Cam-clay and with the swelling model[19]

Model	Node 1		Node 43	
	Displacement U_y (cm)	Convergence U_i (%)	Displacement U_x (cm)	Convergence U_i (%)
Cam-clay	8·01	2·67	7·81	2·6
Swelling	9·5	3·17	8·28	2·76

model, especially at the wall of the gallery. Furthermore, comparisons with the analytical models can be done as the same set of material parameters was considered. As expected, higher displacements were obtained with the strain-hardening models. The values of the final stresses in the clay (Table IV) and of the convergence (Table V) predicted with the swelling model are higher than those obtained with the Cam-clay model; but in both cases the deformed gallery remained

circular. The extent of the plastic domain in the clay determined with both strain-hardening models (Figure 12(a) and (b)) was also wider according to the swelling model.

CONCLUSION

The analysis of the microstructural mechanisms which govern the macroscopic behaviour of the expansive clays was used to propose an elastoplastic rheological model. Thus, the presence of a macroporosity beside a microporosity produces irreversible strains during unloading because of unbalanced repulsive stresses at the scale of the microporosities. This plastic phenomenon during unloading is taken into account by a second yield surface using non-associated plasticity (F_{R-A}) together with a classical contact yield surface (F_C). These two surfaces are in contact by a fixed point, but use independent strain-hardening rules. Thus, for normally consolidated stress states, the variations of the external stresses are balanced by the contact stress variations: the only one activated plastic mechanism corresponds to the surface F_C. On the other hand, for overconsolidated stress states, the variations of the external stresses are totally recovered by the repulsive stresses and the activated plastic mechanism is this of the surface F_{R-A}. The model allows for applying the classical plastic theory using 'loading-unloading' criteria defined from the sign of the plastic multiplier (necessarily positive). Furthermore, no difficulty comes across when using this model in a finite element program to solve boundary problems.

This model well simulates the phenomena observed on the laboratory paths. A first simulation of tunnelling a circular gallery at a great depth in an expansive clay was successfully performed. The results pointed out an increase of the convergence of the gallery and of the plastic areas in comparison with the results obtained with an elastoplastic model of the Cam-clay type. Future work will be devoted to extend this swelling model to partially saturated expansive clays.

REFERENCES

1. G. Didier, B. Soyez, B. Héritier and L. Parez, 'Etude à l'oedomètre du gonflement des sols', *Congrès International sur les sols gonflants*, Dublin (1987).
2. A. Sridharan and M.S. Joyadava, 'Double layer theory and compressibility of clays', *Géotechnique*, **32,** 133–144 (1982).
3. J. K. Mitchel, *Fundamental of Soil Behaviour*, Wiley, New York (1976).
4. A. Sridharan, 'Strength and volume change behaviour of a sand-bentonite mixture', *Canad. Geotech. J.*, **27,** 404 (1990).
5. B. V. Derjaguin and L. Landau, 'Theory of the stability of strongly charged Lyophobic soils and of the Adhesion of Strongly Charged Particles in Solutions of Electrolytes', *Acta Physiochem. USSR*, **14,** 633–662 (1941).
6. E. J. W. Verwey and J. T. G. Overbeek, *Theory of the Stability of Lyophobic Colloids*, Elsevier, Amsterdam (1948).
7. L. Dormieux, P. Barboux and O. Coussy, 'Une modélisation macroscopique du gonflement des argiles saturées' *C.R. Acad. Sci. Séri* II, **256** (1994).
8. L. Börgesson, O. Karnland and L. E. Johannesson, 'Modelling of the physical behaviour of clay barriers close to water saturation', *Engng. Geol.*, **41**(1–4)**,** 127–144 (1993)
9. A. Giraud and G. Rousset, 'Time dependent behaviour of deep clays', *Engng. Geol.*, **41**(1–4)**,** 181–195 (1993).
10. G. Baldi, T. Heckel, A. Peano and R. Pellegrini, 'Development in modelling of the thermo-hydro-geomechanical behaviour of Broom Clay and clay based buffer materials', *Final Report for CEC (FI1W/0150 A)EUR 13365-1 13365-2 EN, ISMES*, Bergamo, Italy (1991).
11. G. Rousset, 'Comportement mécanique des argiles profondes-Application au stockage de déchets radioactifs,' *Ph.D. Thesis*, ENPC, Paris (1988).
12. G. Didier, 'Etude du gonflement cristallin des montmorillonites', *Bull. Groupe Fr. Argiles*, **Tome XXIV,** 99–110 (1972).
13. G. H. Bolt, 'Physico-Chemical analysis of the compressibility of pure clays', *Géotechnique*, **6,** 86–93 (1956).
14. J. N. Israelachvili and G. E. Adams, 'Measurement of forces between two mica surfaces, in aqueous electrolyte solutions in the range 0–100 nm', *J. Chem. Soc.* Faraday Trans. I, **74,** 975–1001 (1978).

15. J. N. Israelachvili, R. M. Pashley, 'Molecular layering of water at surfaces and origin of repulsive hydration forces', *Nature*, **306,** 249–250 (1983).
16. R. Atabek, B. Felix, J. C. Robinet and R. Lahlou, 'Rheological behaviour of saturated expansive clay materials', *Workshop on Stress Partititioning in Engineering Clay Barriers*, Duke University, 29–31 May 1991.
17. J. C. Hujeux, 'Une loi de comportement pour le chargement cyclique des sols', in *Génie Parasismique*, Presses de l'ENPC, V. Davidouci (ed.), 1985, pp. 287–302.
18. R. Lahlou, 'Etude expérimentale d'une argile fortement compactée. Application au stockage des déchets radioactifs', *Colloque René Houpert* '*Structure and mechanical behaviour of geomaterials*', Nancy, 10–11 September 1992, pp. 161–169.
19. S. Tacherifet, 'Modélisation du comportement méchanique des argiles profondes gonflantes, application aux ouvrages de stockages', *Ph.D. Thesis*, University of Orléans, France (1995).

